JOURNAL OF THERMOPHYSICS AND HEAT TRANSFER
Vol. 11, No. 3, July–September 1997

Monitoring Magnetohydrodynamics Boundary Layers Using Emission Line Shape Features

Leslie E. Bauman* and Lihong Zhong†
Mississippi State University, Mississippi State, Mississippi 39762

A strong correlation has been found between the center dip slope of self-reversed atomic potassium emission lines in a coal-fired magnetohydrodynamics flow and the thickness of the cool boundary layer surrounding the hot core flow. The boundary-layer profile was determined indirectly from line shape fitting of simultaneous time-resolved multiwavelength emission and absorption spectra. For line shape fitting, a power law model with an effective boundary-layer width is proposed for modeling the radiative transfer across a turbulent boundary layer, rather than an inverse power law model that is used for a turbulent velocity boundary layer. A simple relationship can be written between the center dip slope and the effective boundary layer width that will allow real-time monitoring of the turbulent flow.

Nomenclature

B = Planck blackbody light intensity
E = particle light extinction-to-absorption ratio
f = fraction
I = light intensity
L = optical path length
N = boundary-layer shape exponent
T = temperature
x = optical path position
z = ratio of blackbody intensity at the particle temperature to blackbody intensity at the gas temperature
α = atomic absorption coefficient, per length
δ = boundary-layer width in power law and inverse power law thermal models
η = particle absorption coefficient, per length
λ = wavelength
τ = optical depth

Subscripts
av = path-averaged temperature
c = core
eff = effective boundary-layer width in the power law model
L = total path length
w = wall
x = path position
λ = wavelength dependence

Introduction

EMISSION spectra from high-temperature flows, flames, rocket plumes, etc., provide line-integrated information about the state of the flow, in particular, the temperature and the emitting species density. For highly symmetric flows, emission profiles along various chords of a flow have been used with Abel inversion to indirectly extract profiles of temperature and species density from the emission spectra. For the most part, the line-integrated nature of emission spectra is considered a disadvantage and is used as an argument for the use of spatially resolved laser-based spectroscopic measurements. For confined flows with limited optical access, obtaining spatial information can only be accomplished with traversing and consequent lack of time resolution. For a highly fluctuating flow, spatial information obtained indirectly from time-resolved multiwavelength emission spectra may provide a truer picture of the flow properties than direct but time-averaged spatially resolved measurements.

Recent magnetohydrodynamic (MHD) power generation development has centered on coal-fired combustion flow seeded with potassium as a source of conduction electrons. Previous work has demonstrated that line shape fitting of simultaneous potassium D-line emission and absorption spectra can provide thermal boundary-layer information on the high-temperature flow.[1] Such experimental measurements provide information important for process analysis and accurate modeling of the heat transfer and electrical conduction.[2] With multiwavelength detection, the boundary-layer information is obtained from a spectrum representing a snapshot of the flow, and probability distribution functions can be developed from analysis of multiple spectra to reveal the fluctuations in the flow. Although line shape fitting can provide this information, the fitting is too slow to be used as a commonplace diagnostic, and a study was undertaken to find correlations between experimental line shape features and the flow parameters to find a method for real-time monitoring of the turbulent boundary-layer flow.

Line Shape Fitting

Figure 1 illustrates potassium D-line emission spectra from a channel-simulation subsection of a prototype-scale MHD facility.[3] The nominal test conditions were combustion of western air with 1% potassium seed added as a 47% solution of potassium carbonate, 0.85 primary, and 1.10 secondary stoichiometry. The combustor provided 100% slag carryover. The optical ports were located 0.5 m downstream from the combustor where the pipe diameter, and therefore, optical path length, is 12 cm and the pressure was estimated as 1.78 atm. The potassium lines are very broad because of high potassium loading and high temperature combined with a long optical path length, and are deeply self-reversed because of the cool boundary layer surrounding the hot core flow. The dramatic differences in line shape indicate large fluctuations in flow parameters, particularly the boundary-layer width.

Fitting the potassium emission and absorption line shapes to a radiative transfer model allows an indirect determination of the thermal profile across the MHD channel flow. The absorp-

Presented as Paper 95-1968 at the AIAA 26th Plasmadynamics and Lasers Conference, San Diego, CA, June 19–22, 1995; received Jan. 14, 1997; revision received March 24, 1997; accepted for publication March 25, 1997.

*Professor, Department of Physics and Astronomy, P. O. Box 5167. E-mail: Bauman@photon.dial.msstate.edu. Member AIAA.
†Ph.D. Student, Engineering Physics, P.O. Box 5167.

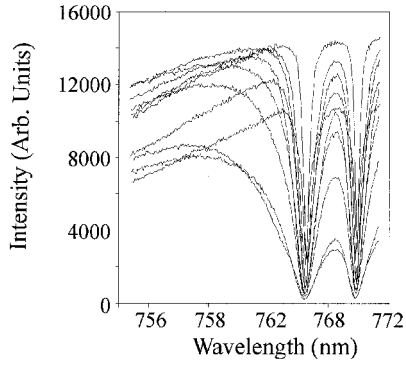

Fig. 1 Example potassium D-line emission spectra. Each spectrum is an 0.5-ms time exposure with an interval of 1 s between the consecutive spectra.

tion spectrum must be included in the fit along with the emission spectrum and because of the high speed and large fluctuations in the flow, they must be recorded simultaneously.[4] The fitting is accomplished using a nonlinear least-squares algorithm modeling the line shape as reported previously,[1] and summarized briefly here.

The atomic *D*-line emission absorption spectra are modeled at each wavelength by an optical path integral across the flow as

$$I_\lambda(L) = e^{-\tau_L}\int_0^L (\alpha_\lambda + z\eta)B_\lambda(T_x)e^{\tau_x}\,\mathrm{d}x + I_\lambda(0)e^{-\tau_L}$$
$$\tau_x = \int_0^x (\alpha_\lambda + \eta E)\,\mathrm{d}x' \tag{1}$$

Here, $I_\lambda(0)$ is the incident reference lamp signal and $I_\lambda(L)$ is the outgoing light from the flow at a path length of L. Light scattered into the optical path by particles is not included in the model. The emission-only intensity is found by setting $I_\lambda(0)$ to zero. The atomic absorption coefficient α_λ is a function of the path position x through its dependence upon temperature and density, and it is modeled by a Voigt profile matched to a power law profile in the line wings.[5]

Broadband particle cloud effects are included as ηE and $z\eta$.

A single parameter model for the potassium atom density profile as a function of temperature was developed from chemical equilibrium predictions for conditions representative of an MHD flow. In this model the number density is related to the density at the core temperature through an exponential function that can vary smoothly between an ideal gas law relationship and equilibrium chemistry. The four-temperature profile model parameters given next: two atomic density parameters and two particle cloud parameters constitute the eight parameters used in the fitting routine.

Figures 2–5 illustrate the results of fitting over 6000 spectra recorded over a several hour period to a model thermal boundary-layer profile as discussed later in this paper. Results reported in a previous paper show that the core temperature is well determined and the value compares well to a modified line reversal measurement that was used as the starting value for fitting.[1] The near-wall temperature is found from a Planck blackbody averaging across a narrow portion (0.5 mm) of the fit thermal boundary-layer profile near the wall.

The probability distribution function for the boundary-layer width shows a sharp peak with the most probable boundary-layer width just under 1 cm. A significant number of samples with very wide boundary layers are also predicted. An average of the thermal profiles determined by fitting the instantaneous line shapes predicts a boundary-layer width of about 2.5 cm, which matches that found with time-averaged traversing measurements of velocity by laser-Doppler velocimetry (LDV) and

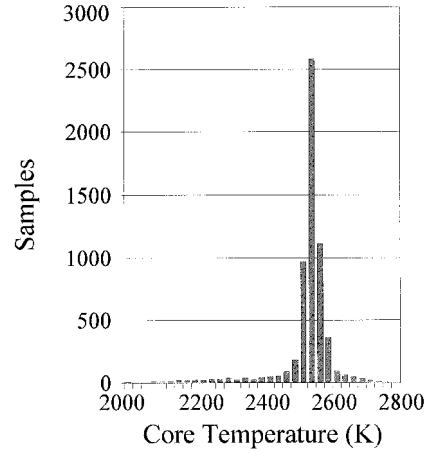

Fig. 2 Sample distribution for the MHD flow core temperature found from line shape fitting.

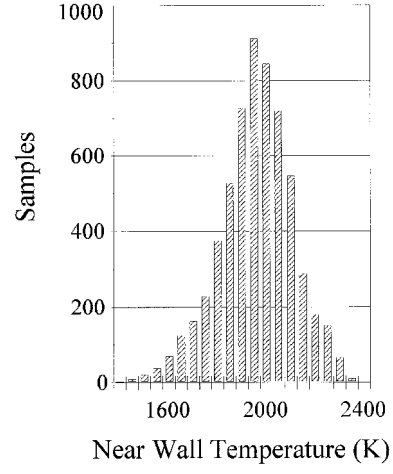

Fig. 3 Sample distribution for the MHD flow near-wall temperature found from line shape fitting.

measurements of temperature by coherent anti-Stokes Raman spectroscopy (CARS). The results found from time-resolved line shape fitting more closely match flow modeling predictions of a narrow boundary layer.[6]

Thermal Boundary-Layer Model Profiles

The typical thermal boundary-layer model used for turbulent flow and that used for the fitting results shown earlier are given by an inverse power law model as

$$T_x = \begin{cases} T_w + (T_c - T_w)\left(\dfrac{x}{\delta}\right)^{1/N} & 0 \le x \le \delta \\ T_c & \delta < x < L - \delta \\ T_w + (T_c - T_w)\left(\dfrac{L-x}{\delta}\right)^{1/N} & L - \delta \le x \le L \end{cases} \tag{2}$$

where L is the pipe flow diameter that corresponds to the optical path length across the flow. This inverse power law model is taken from that for a turbulent velocity profile, assuming that the Prandtl number is not far removed from 1 (Ref. 7). For turbulent boundary layers, N is typically 7–10.

Example fits to two spectra using the inverse power law profile are shown in Figs. 6 and 7 along with the fit temperature profile parameters and uncertainties. The uncertainties are estimated by the fitting parameter curvature matrix. Typical uncertainties in fitting the wall temperature were 200–300 K. The inverse power law profiles are very steep at the wall and

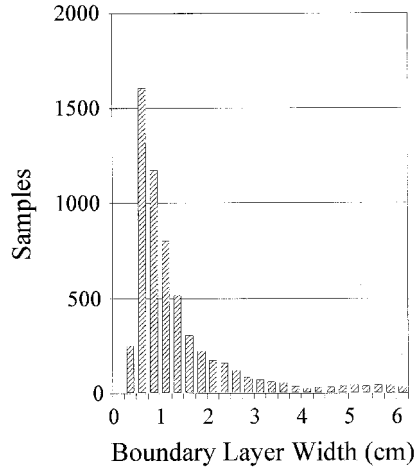

Fig. 4 Sample distribution for the MHD flow boundary-layer width found from line shape fitting. The total optical path length in the duct is 12 cm.

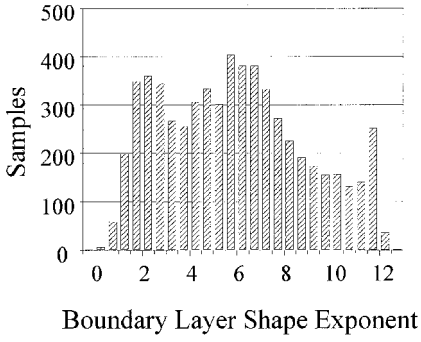

Fig. 5 Sample distribution for the MHD flow boundary-layer shape exponent.

typically yielded unreasonably low values for the wall temperature. The physically reasonable fitting results shown earlier for the near-wall temperature were found by integrating the thermal profiles from the wall inward to a distance of 0.5 mm.

Because the inverse power law profile is exceedingly steep at the wall, it is not well behaved for numerical integration and does not provide a true measure of the wall temperature. We propose to model the radiative transfer instead with a power law form for the thermal boundary-layer profile as given by

$$T_x = \begin{cases} T_c - (T_c - T_w)\left(\dfrac{\delta - x}{\delta}\right)^N & 0 \le x \le \delta \\ T_c & \delta < x < L - \delta \\ T_c - (T_c - T_w)\left[\dfrac{x - (L - \delta)}{\delta}\right]^N & L - \delta \le x \le L \end{cases} \tag{3}$$

For the same four parameters, T_c, T_w, δ, and N, the two models have the same average temperature in the boundary layer, $T_{av} = (T_w + NT_c)/(1 + N)$. However, the alternate model is less steep at the wall, and so it is better behaved for the numerical integrations needed for the fitting.

The inverse power law profile has a distinct kink in the profile, where it matches the core value, whereas the alternate profile matches smoothly to the core temperature at the edge of the boundary layer. As a consequence, the power law model does not provide as distinct a boundary-layer width as the inverse power law profile. We suggest the computation of an

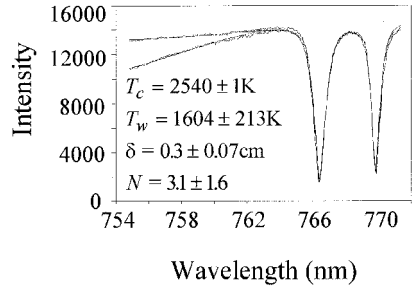

Fig. 6 Illustration of line shape fitting results for an example spectrum that fits to a thin boundary layer.

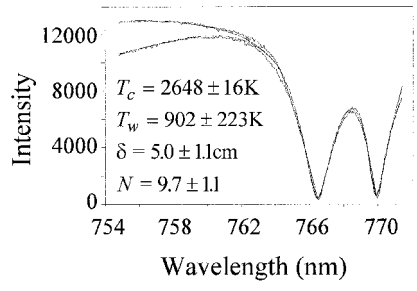

Fig. 7 Illustration of line shape fitting results for an example spectrum that fits to a wide boundary layer.

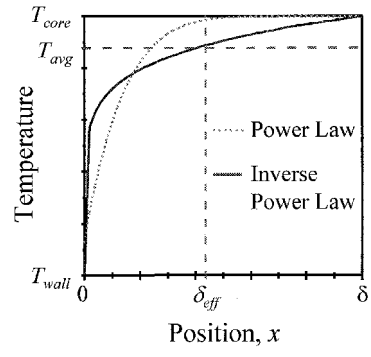

Fig. 8 Comparison of the inverse power law and power law thermal boundary-layer models for $N = 7$.

effective boundary-layer width, defined as the spatial position where the temperature is a fraction f of the difference between the wall and core temperature as

$$\delta_{\text{eff}} = [1 - (1 - f)^{1/(N+1)}]\delta \tag{4}$$

where f was taken to be 0.99 for the following computations. Figure 8 illustrates the difference between the two model profiles.

A subset of 50 emission/absorption spectra were fit to a boundary-layer profile using the inverse power law model and the alternate power law model as presented earlier. Little difference was seen between fitting parameters for the two models, comparing the sum of the square deviations, the spatially averaged temperature and the core temperature for each. Figure 9 shows a comparison between the two model thermal boundary-layer profiles for a spectrum showing a narrow boundary-layer profile. The excellent agreement between the effective boundary-layer width found with the power law model and the boundary-layer width of the inverse power law model is also illustrated.

Not all of the fit profiles compare quite so favorably, especially those for the spectra that fit to larger boundary-layer widths, an example is shown in Fig. 10. However, the fits closely predict the boundary-layer widths, for this example, δ

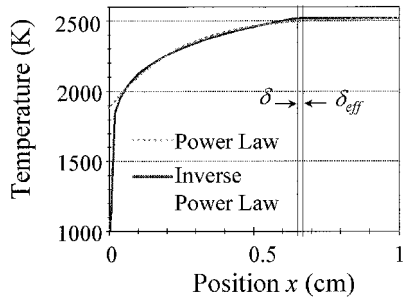

Fig. 9 Comparison of the thermal profiles found from fitting for an example spectra fit to a narrow boundary layer.

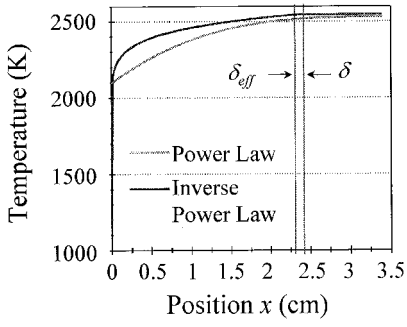

Fig. 10 Comparison of the thermal profiles found from fitting for an example spectra fit to a relatively wide boundary layer.

= 2.4 and δ_{eff} = 2.3 cm, for the inverse power law and power law thermal profiles, respectively.

There was no significant difference in the sum of the square deviations found by fitting this particular emission absorption spectrum to the two model profiles, but the core temperatures found from the two fits differed by 20 K. This is a general result for those spectra with broad center dips. Perhaps these spectra do not contain enough spectral information on the wings of the line to nail down the core temperature and fit to a unique boundary-layer profile. For the 50 spectra, the sum of the square deviations between the core temperature found for the two models was 6 K for the spectra with boundary layer widths less than 1.5 cm and 23 K for all of the spectra.

Figure 11 shows a comparison between the boundary-layer width found from an inverse power law profile and the effective boundary-layer width from a power law profile. Only at the larger widths is there a systematic difference between the two model results, and then the effective boundary-layer width using a power law model predicts more narrow boundary layers widths than the inverse power law model.

The sample distribution for the boundary-layer widths found from fitting to the two different models is shown in Fig. 12. Both models predict that the boundary-layer width for this flow at this time to be most probably between 1–1.5 cm.

There is a general tendency for the wall temperature found with the power law profile to be lower than that found for the near-wall temperature and the inverse power law profile as shown in Fig. 13. The wall temperature found by fitting to a power law profile has an average value of 1855 ± 111 K, and agrees well with a typically assumed value of 1800 K for slag-coated walls.[2]

The average near-wall temperature found from the inverse power law was 1951 ± 166 K. The near-wall temperature is a mathematical attempt to estimate the wall temperature by integrating the very steep thermal profiles over a small arbitrary amount (0.5 mm). Although a rough estimate could be made of the wall temperature from the inverse power law fits, it seems more satisfying to find the wall temperature more directly by fitting to the power law profile. The wall temperature would not be expected to fluctuate as rapidly as the gas

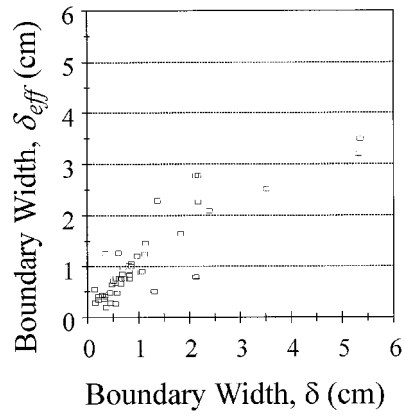

Fig. 11 Comparison of the boundary-layer widths found by fitting to model thermal profiles: δ and δ_{eff} for inverse power law and power law models, respectively.

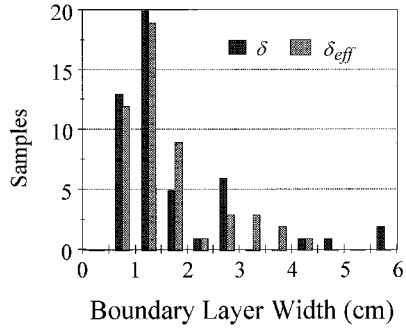

Fig. 12 Frequency distribution of boundary-layer widths found by fitting to the two model thermal profiles.

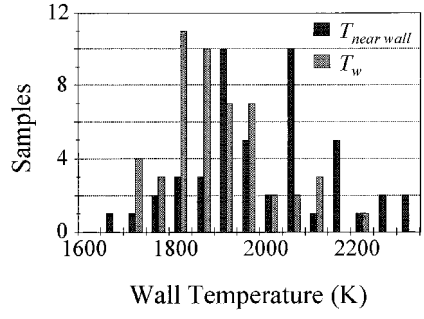

Fig. 13 Frequency distribution wall temperatures found by fitting to the two model thermal profiles.

temperature, and so the smaller uncertainty limit also implies a better determination of the wall temperature with this profile.

Line Shape Features and Correlations

The same 50 emission/absorption spectra were investigated for correlations between line shape and the boundary-layer profile parameters. Figure 14 illustrates the simple shape features that were calculated for each emission spectrum: the slope of the intensity on the line wing, the slope of the intensity in the center dip at a half-maximum intensity, the wavelength of maximum intensity and the value of the maximum, and the center dip intensity.

A strong correlation was seen between the boundary-layer width and the slope in the center dip. Figure 15 shows the data and a model relationship between the relative slope, $(\Delta I/\Delta\lambda)/I_{max}$, and the effective boundary-layer width from a power law profile fit. The points are well fit to a curve of the form $a + be^{cx}$, as shown. The form of the curve is simply that which gave the best fit without regard to theoretical analysis. Similar

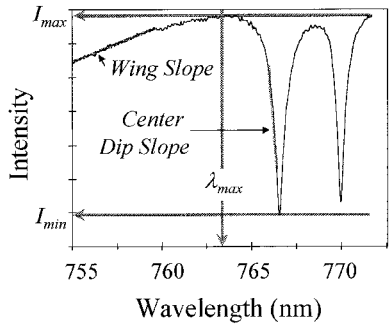

Fig. 14 Illustration of self-reversed emission line shape features.

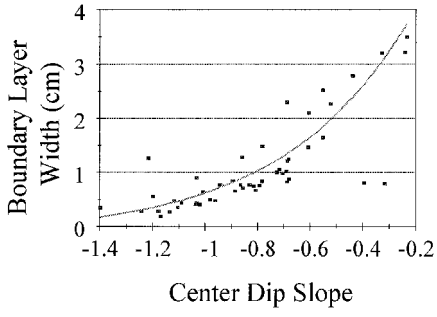

Fig. 15 Boundary-layer width δ_{cm} as determined by line shape fitting vs the center dip slope.

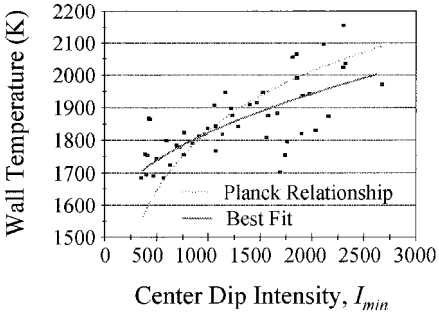

Fig. 16 Wall temperature found by line shape fitting vs the center dip intensity.

curves could be drawn for the boundary-layer width found by fitting to an inverse power law model.

The particle parameters, $z\eta$ and ηE, determined from fitting, were quite variable presumably because of large fluctuations in the particle loading. The average for all fits corresponds to a particle cloud optical depth of 0.6, a value that reduces the transmitted lamp intensity by half across the optical path length of the flow.[1] The broadband particle cloud affects the spectral line shape significantly only in the line wings.[8] Near line center the absorption coefficient is dominated by the atomic absorption coefficient, and the shape of the center dip is fundamentally determined by temperature and atomic density profiles. Hence, the correlation between the center dip slope and the boundary-layer width is not directly affected by the particle loading in the flow. However, the particle cloud does affect the radiative transfer and will indirectly affect this correlation through the actual thermal profile. The empirical form for the relationship between boundary-layer width and center dip slope can only be assumed valid for the nominal flow conditions for which the line shape analysis was performed.

A reasonable correlation was also found between the center dip intensity I_{min} and the wall temperature as shown in Fig. 16. This was expected because at line center the flow is optically thick and the emitted light arises only from a narrow outer layer of the flow. The curve found as a best fit to the data by least-square fitting is flatter than that expected by purely a Planck blackbody relationship. This may be because of the spectral resolution of the spectrometer and the consequent convolution of higher intensity data away from line center into this spectral feature.

One other line shape feature of particular interest was the wavelength of maximum intensity, since it had been suggested that this feature could provide a real-time monitor of the potassium density if one had an estimate the thermal boundary-layer width.[9] We found no correlation between this feature and the potassium density as found by the emission absorption measurements on the line wings and by line shape fitting. This is most likely a result of the extreme fluctuations in boundary-layer width in the coal-fired flow and may not apply to other more stable flows, such as natural gas combustion MHD flows.

Conclusions

Previous results showed that emission/absorption line shape fitting to an inverse power law model of a thermal boundary-layer profile could provide a good measure of the core temperature, the boundary-layer width, and the average or bulk temperature in a high-temperature, turbulent MHD flow. However, the shape of the boundary-layer profile was not as well determined and the wall temperature could only be estimated by a mathematical artifice.

In this study, a power law model has been suggested for the shape of the thermal boundary-layer profiles rather than an inverse power law model. The less steep slope at the wall for this model allows for 1) a better determination of the wall temperature and 2) use of larger step sizes in the numerical integration, and hence, faster fitting. The apparent tradeoff in information between boundary-layer width and wall temperature is avoided by using an effective boundary layer width that varies with the power law exponent.

A strong correlation was found between the slope of the emission intensity in the center dip region and the boundary-layer width found by line shape fitting to a power law model of the thermal profile. The empirical form for the relationship between the boundary-layer width at the particular flow conditions will allow a real-time monitor of the boundary-layer width in this high speed flow. While these results are specific to the flow conditions in the particular MHD flow, a similar form could be derived for other boundary-layer flows by the same method used in this study.

It was also found that the center dip intensity is roughly correlated with the wall temperature. A monitor based upon this emission feature could be useful for avoiding operating the channel electrodes or sidewalls at temperatures higher than design, or for early detection of water leaks that would show up as cool wall temperatures. Both of these line shape features are easily monitored in real time so that a simple emission spectroscopy system with fiber optic access to an MHD channel could provide a simple and robust diagnostic to assist in process monitoring and control. The analysis techniques presented here are not limited to only MHD flows, but could certainly be adapted as needed and applied to other boundary-layer flows using an appropriate self-reversed emission line.

Acknowledgments

This work was supported by National Science Foundation Grant CTS-9411150. The potassium spectra were recorded during experiments sponsored by U.S. Department of Energy Contract DE-AC02-80ET15601.

References

[1]Bauman, L. E., "Investigation of MHD Flow Structure and Fluctuations by Potassium Lineshape Fitting," *Combustion and Flame*, Vol. 98, Nos. 1/2, 1994, pp. 46–58.

[2]Im, K. H., and Ahluwalia, R. K., "Heat and Mass Transfer in MHD Channels," *Journal of Energy*, Vol. 5, No. 1, 1981, pp. 22–30.

[3]Chapman, J. N., Johanson, N. R., and Attig, R. C., "HRSR Results from Preliminary Tests on Montana Rosebud Coal," *Proceedings of the 30th Symposium on Engineering Aspects of MHD*, SEAM, Inc., Session XIII, Paper 1, Univ. of Tennessee Space Inst., Tullahoma, TN, 1992, pp. 1–9.

[4]Bauman, L. E., Wang, W., Luthe, J. C., and Kumar, R. A., "Measurements of Temperature and Seed Atom Density in High-Speed MHD Flows," *Journal of Thermophysics and Heat Transfer*, Vol. 8, No. 3, 1994, pp. 473–477.

[5]Bauman, L. E., "Potassium D-Line Blue Wing Absorption Coefficient Under Combustion-Fired MHD Conditions," *Journal of Thermophysics and Heat Transfer*, Vol. 7, No. 1, 1993, pp. 25–29.

[6]Wilson, W. W., Singh, J. P., Yueh, F. Y., Bauman, L. E., George, A., and Cook, R. L., "Comparison of Velocity and Temperature Measurements in an MHD Topping Cycle Environment with Flow Field Model Calculations," *Combustion Science and Technology*, Vol. 109, 1995, pp. 1–22.

[7]Kays, W. M., and Crawford, M. E., *Convective Heat and Mass Transfer*, McGraw–Hill, New York, 1980.

[8]Bauman, L. E., Luthe, J. C., and Ma, X., "An Emission Absorption Technique Suitable for Automatic Measurement of Seed Atom Density in Coal-Fired MHD Flows," *Magnetohydrodynamics: An International Journal*, Vol. 3, No. 1/2, 1992, pp. 43–53.

[9]Balashov, N. A., Vasil'eva, I. A., Gaponov, I. M., Deputatova, L. V., Zykova, N. M., Kirillov, V. V., Malyuzhonok, G. P., Mikhailov, Y. S., Nedospasov, A. V., Nefedov, A. P., Novosadov, V. B., Petrov, K. N., Poberezhskii, L. P., Tolchinskii, L. S., Urinson, A. S., Shapiro, I. G., and Shumyatskii, B. Y., "Plasma Diagnosis on the U-25," *High Temperature*, Vol. 12, No. 1, 1974, pp. 359–364.